Proceedings of 20th International Congress on Acoustics, ICA 2010

23-27 August 2010, Sydney, Australia

Underwater sound radiation by a layered infinite elastic plate with discontinuity

Yanni Zhang (1), Jie Pan (1) and Darryl McMahon (2)

(1) School of Mechanical Engineering, , University of Western Australia, Crawley WA Australia,
(2) DSTO, HMAS Stirling, Rockingham WA 6958

PACS: 43.40.Rj

ABSTRACT

The underwater sound radiation from layered structure is determined by the properties of elastic waves in the structure and by interaction between structural/structural waves and between structural/fluidal waves. In this paper, a model of a layered infinite plate is used to address how the properties and interaction influence the near field and far field characteristics of the radiated sound. In particular, the effect of structural discontinuity introduced to the layered plate by a finite signal conditioning plate on underwater sound radiation is investigated. The scattering of structural waves in the layered plate by the signal conditioning plate is used to explain the changes in the radiated sound due to the discontinuity.

INTRODUCTION

The addition of compliant layers such as elastic foam attached to the outside surface of an underwater structure is a common approach to reduce the self-noise from the structural vibration and the reflection of incoming signals from active sonors [1-4]. Ko et al. [1] investigated the reduction of sound radiation by a base plate covered by an air-voided elastomer using the elasticity theory. He found that the shear wave speed and related loss factor have negligible effects on the noise reduction. Keltie [2] simplified Ko's model using the thin plate theory for the base plate. Latter Berry et al. extended the problem to a finite rectangular plate using a locally reactive model [3] and a modified 3D model [4] with the shearing wave neglected as well after checking Ko's observation for finite plate.

The consideration of the effect of discontinuity on the surface of the elastic foam, which is the interface between water and the layered structure, on the sound radiation of the overall structure comes from a proposal of introducing a signal condition plate on the surface. As the foam absorbs incoming sound, a locally placed plate with small sound absorption on the surface may increase the local signal to noise ratio of the incoming sound for a detecting hydrophone placed in front of the plate.

This raises a general question of how sound is radiated by a coated elastic plate with inhomogeneity, which however, received little attenuation because of the complexity of interaction between elastic waves in the foam (coupled with base plate and fluid) and the structural inhomogeneity (such as the signal conditioning plate). Previous studies mainly focused on vibro-acoustic response of a single elastic plate with discontinuity [5-10]. Most of them utilized classical plate theory [8, 9] with discontinuity treated as a concertrated mass. In order to be applied to broader frequency range, Seren et al. [5] presentd redults of sound radiation of insonified elastic plate with a line discontinuity, such as a ractanular rib, based on Mindlin's plate theory. Pathak et al. [6] further extended/freed the frequency range for a line discontinuity on the vacuum side by appling 2D elasticity. Cuschieri and Feit [7] used Green function methods based on the thin plate theory and calculated the near-field sound with a specific emphasis on the method. Then they considered the scattering effects of distributed inhomogeneity on the far- and near-field of elastic plate [8, 9]. Later DiPerna and Feit [10] obtained the analytical solution for the response of a in-vacuo thin plate with (discrete) mass discontinuity(ies) using perturbation technique.

In this paper, we present an analytical model of underwater sound radiation from an infinite panel covered by elastic foam. In particular the model includes the scattering of elastic waves in the foam by a finite signal conditioning plate. The study focuses on the effect of such wave scattering on the far field directionality of the radiated sound and near field pressure distribution. The vibration distribution in the elastic foam (due to the scattering) is also analysed to explain the changes in the radiated sound when the signal conditioning plate is introduced. Effects of structural parameters such as the dimensions of the signal conditioning plate and material properties of the foam on radiated sound are also investigated.

MODELING OF THE LAYERED PLATE

A sketch of the layered plate of infinite size is shown in Figure. 1. The base plate of thickness h and density ρ, and the elastic foam of thickness h_1 and density ρ_1 are located below the surface $z=0$. A stationary fluid with density ρ_0 and sound speed c_0 occupies space above the elastic form. In vacuum condition is assumed for the medium below the base plate. A finite signal conditioning plate of thickness h_2 and density ρ_2 is placed on the top surface of the elastic foam. The layered plate is excited by a line homonic force in the form of $F\delta(x-x_o)e^{j\omega t}$ at the bottom of the base plate ($z=-h-h_1$) and in the direction of z. For convenience, the time harmonic dependence ($e^{j\omega t}$) for all field variables is suppressed from this point.

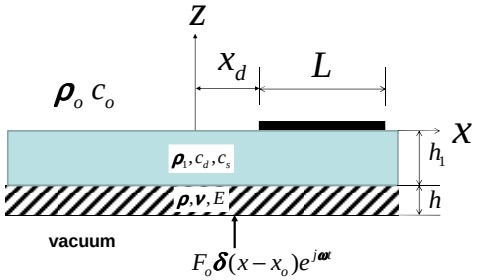

Figure 1. The layered plate with a finite signal conditioning plate as a discontiuity

The external loading to the layered plate includes the normal and tangential forces (per unit area) acting on the top of the foam by the fluid pressure and stress between the foam and the signal conditioning plate. Another external loading is on the base plate and in the z direction, representing the force from machinery attached to the layered plate. This force pwer unit area is denoted as $F_o\delta(x-x_o)$.

The equation of motion governing the transverse displacement $w_h(x)$ of the base plate is [11]

$$(D_1\frac{\partial^4}{\partial x^4}-\omega^2\rho h)w_h(x)=\sigma_z(x,-h_1) +\frac{h}{2}\frac{\partial\tau_{zx}(x,-h_1)}{\partial x}+F_o\delta(x-x_o) \tag{1}$$

where $D_1=E_1h^3/12(1-v_1^2)$ is the bending stiffness of the base plate with Young's Modulus E_1 and Poisson's ratio v_1. σ_z and τ_{zx} are respectively the normal and shear stress components in the elastic foam..

The in-plane longitudinal displacement $u_h(x)$ is described as [12]

$$(E_1^{'}h\frac{\partial^2}{\partial x^2}+\rho h\omega^2)u_h(x) =\frac{-v_1h}{2(1-v_1)}\frac{\partial[(\sigma_z(x,-h_1)+F(x)]}{\partial x}-\tau_{zx}(x,-h_1) \tag{2}$$

Where $E_1^{'}=E_1/(1-v_1^2)$ 。

The elastic waves in the foam are modelled using 2D elastic solid theory [13] and sound pressure in the fluid is described by 2D sound wave equation. They are summarized as

$$(\frac{\partial^2}{\partial x^2}+\frac{\partial^2}{\partial z^2})\varphi(x,z)=-\frac{\omega^2}{c_d^2}\varphi(x,z) \tag{3}$$

$$(\frac{\partial^2}{\partial x^2}+\frac{\partial^2}{\partial z^2})\psi(x,z)=-\frac{\omega^2}{c_s^2}\psi(x.z) \tag{4}$$

$$(\frac{\partial^2}{\partial x^2}+\frac{\partial^2}{\partial^2 z})p(x,z)=-\frac{\omega^2}{c_o^2}p(x,z) \tag{5}$$

Where ϕ and ψ are the dilatational and the shear wave (also called the scalar potential and vector potential), and c_d, c_s and c_0 are dilatational and shear wave speed and the speed of sound in the fluid, respectively. $p(x,z)$ is the sound pressure in the fluid.

The scalar and vector potential and sound pressure can be written as inverse wavenumber transformation.

$$\phi(x,z)=\frac{1}{2\pi}\int_{-\infty}^{+\infty}\Phi(k,z)\mathrm{e}^{-ikx}dk \tag{6}$$

$$\psi(x,z)=\frac{1}{2\pi}\int_{-\infty}^{+\infty}\Psi(k,z)\mathrm{e}^{-ikx}dk \tag{7}$$

$$p(x,z)=\frac{1}{2\pi}\int_{-\infty}^{+\infty}P(k,0)\mathrm{e}^{-jkx-\alpha_0 z}dk \tag{8}$$

where $\alpha_0=\sqrt{k^2-k_0^2}$ represents the acoustic wavenumber in the *z* direction. The normal and tangential displacements and stresses in the foam are related to the scalar and vector potentials based on reference [13].

It is noted that the displacements of the signal conditioning plate are equal to those of the foam at its interface with the plate as the thin plate model is used for the vibration of the signal conditioning plate.

The force equilibrium and displacement continuity requirements at all the interfaces are.

(a) $z=-h_1$

$$w_h(x)=u_z(x,z=-h_1) \tag{9}$$

$$u_h(x)-\frac{h}{2}\frac{\partial w_h(x)}{\partial x}=u_x(x,z=-h_1) \tag{10}$$

$$\sigma_z(x,-h_1)=(D_1\frac{\partial^4}{\partial x^4}-\omega^2\rho h)w_h(x) -\frac{h}{2}\frac{\partial\tau_{zx}(x,-h_1)}{\partial x}-F_o\delta(x-x_o) \tag{11}$$

$$\tau_{zx}(x,-h_1)=-(E_1^{'}h\frac{\partial^2}{\partial x^2}+\rho h\omega^2)u_h(x) -\frac{v_1h}{2(1-v_1)}\frac{\partial[(\sigma_z(x,-h_1)+F(x)]}{\partial x} \tag{12}$$

(b) $z=0$

(i) $x_d>x>x_d+L$

$$\sigma_z(x,0)=-p(x,0) \tag{13}$$

$$\tau_{zx}(x,0)=0 \tag{14}$$

$$u_z(x,0) = \frac{1}{\rho_o \omega^2} \frac{\partial p(x,z)}{\partial z}\bigg|_{z=0} \tag{15}$$

(ii) $x_d < x < x_d + L$

$$w_s(x) = u_z(x,0) \tag{16}$$

$$u_s(x) + \frac{h_2}{2}\frac{\partial w_s(x)}{\partial x} = u_x(x,0) \tag{17}$$

$$\sigma_z(x,0) = -p(x,0) + (\rho_2 h_2 \omega^2 - D_2 \frac{\partial^4}{\partial x^4}) w_s(x) + \frac{h_2}{2}\frac{\partial \tau_{zx}(x,0)}{\partial x} \tag{18}$$

$$\tau_{zx}(x,0) = (E_2^{'} h_2 \frac{\partial^2}{\partial x^2} + \rho_2 h_2 \omega^2) u_s(x) + \frac{v_2 h_2}{2(1-v_2)}\frac{\partial[\sigma_z(x,0) - p(x,0)]}{\partial x} \tag{19}$$

(c) $z = h_2 \cong 0$

$$w_s(x) = \frac{1}{\rho_o \omega^2}\frac{\partial p(x,0)}{\partial z} \tag{20}$$

where u_z and u_x are the normal and tangential displacements of the foam. w_s and u_s are the transverse and longitudinal displacements of the signal conditioning plate. $D_2 = E_2 h_2^3 / 12(1-v_2^2)$ is the bending stiffness of the signal conditioning plate with Poisson's ratio v_2 and Young's modulus E_2. L and x_d are the length and offset of the signal conditioning plate.

Substituing Equaitons (9) and (10) into Equations (11) and (12) gives

$$\sigma_z(x,-h_1) = (D_1 \frac{\partial^4}{\partial x^4} - \omega^2 \rho h) u_z(x,-h_1) - \frac{h}{2}\frac{\partial \tau_{zx}(x,-h_1)}{\partial x} - F_o \delta(x - x_o) \tag{21}$$

$$\tau_{zx}(x,-h_1) = -(E_1^{'} h \frac{\partial^2}{\partial x^2} + \rho h \omega^2) u_x(x,-h_1) - \frac{v_1 h}{2(1-v_1)}\frac{\partial[(\sigma_z(x,-h_1) + F(x)]}{\partial x} \tag{22}$$

Substituting Equations (16) and (17) into Equations (18) and (19) and combining Equaitons (18) and (19) with Equation (13) and (14) lead to

$$\sigma_z(x,0) = -p(x,0) + [(\rho_2 h_2 \omega^2 - D_2 \frac{\partial^4}{\partial x^4}) u_z(x) + \frac{h_2}{2}\frac{\partial \tau_{zx}(x,0)}{\partial x}]\Delta H(x) \tag{23}$$

$$\tau_{zx}(x,0) = \{(E_2^{'} h_2 \frac{\partial^2}{\partial x^2} + \rho_2 h_2 \omega^2)[u_x(x,0) - \frac{h_2}{2}\frac{\partial u_z(x)}{\partial x}] + \frac{v_2 h_2}{2(1-v_2)}\frac{\partial[\sigma_z(x,0) - p(x,0)]}{\partial x}\}\Delta H(x) \tag{24}$$

where $\Delta H(x) = H(x - x_d) - H(x - x_d - L)$ is the window function of unit amplitude at x where the signal conditioning plate is placed. H is the Heaviside step function.

Because of Equation (16), Equations (15) and (20) allow the expression of the radiated sound pressure using the normal velocity component $u_z(x,0)$ of the elastic foam in the entire range of ($x, z = 0$).

The stress and displacement components of the foam in Equations (21), (22), (23) and (24) are expressed by coefficients of velocity potentials A_1, B_1, A_2 and B_2 [1].

Combing Equations (21), (22), (23) and (24) with Equaton (15) and transforming them into the wavenumber domain with respect to x , a matrix equation with unknowns [A_1 , B_1 , A_2 , B_2]is obtained as

$$[T]\begin{bmatrix} A_1 \\ B_1 \\ A_2 \\ B_2 \end{bmatrix} = \begin{bmatrix} F_o e^{jkx_0} \\ 0 \\ P_z(k,0) \\ P_x(k,0) \end{bmatrix} \tag{25}$$

where the coefficient matix $[T]$ is listed in the appendix and the wavenumber coupling terms due to the wave scattering by the signal conditioning plate are

$$P_z(k,0) = \frac{1}{2\pi}\int_{-\infty}^{+\infty} [\frac{jk' h_2 \rho_1 c_s^2 (k^2 - \beta^2)}{2} \{[\alpha(\rho_2 h_2 \omega^2 - D_2 k'^4) - k'^2 h_2 \rho_1 c_s^2 \alpha] B_1 - jk'(\rho_2 h_2 \omega^2 - D_2 k'^4)] A_2\} g(k - k') dk' \tag{26}$$

$$P_x(k,0) = \frac{1}{2\pi}\int_{-\infty}^{+\infty} -\frac{jk' v_2 h_2}{2(1-v_2)} [\rho_1 c_s^2 (k^2 - \beta^2) A_1 - 2j\rho_1 c_s^2 k \beta B_2 + \frac{\rho_o \omega^2}{\alpha_0}(\alpha B_1 - jk' A_2)]\} g(k - k') dk' \tag{27}$$

where $g(k) = \int_{-\infty}^{+\infty} \Delta H(x) e^{jkx} dx = L e^{jk(x_d + \frac{L}{2})} \sin c(k\frac{L}{2})$ is the wavenumber transformation of window function $\Delta H(x)$. If these coupling terms become zero as $L = 0$ or $h_2 = 0$, then each wavenumber component of the layered plate is only excited by the corresponding forcing component ($F_o e^{jkx_0}$) only. The problem becomes a homogeneous layered plate with a base plate covered by elastic foam without signal conditioning plate.

Hence the normal displacement of the foam is

$$U_z(k,z) = [T^n]\begin{bmatrix} A_1 \\ B_1 \\ A_2 \\ B_2 \end{bmatrix} \tag{28}$$

where

$$[T^n] = [-\alpha \sin(\alpha z), \alpha \cos(\alpha z), -ik \cos(\beta z), -ik \sin(\beta z)] \tag{29}$$

The sound pressure in the fluid is expressed as

$$p(x,z)=\frac{1}{2\pi}\int_{-\infty}^{+\infty}P(k,0)e^{-jkx-\alpha_0 z}dk$$

$$=-\frac{\rho_o\omega^2}{2\pi}\int_{-\infty}^{\infty}\frac{U_z(k,0)}{\alpha_0}e^{-jkx-\alpha_0 z}dk\ . \quad (30)$$

Equation (25) allows A_1, B_2 to be calculated by A_2, B_1 as follows:

$$A_1(k)=K_{10}(k)+K_{11}(k)B_1(k)+K_{12}(k)A_2(k) \quad (31)$$

$$B_2(k)=K_{20}(k)+K_{21}(k)B_1(k)+K_{22}(k)A_2(k) \quad (32)$$

where functions $K_{10}(k)$, $K_{11}(k)$, $K_{12}(k)$, $K_{20}(k)$, $K_{21}(k)$ and $K_{22}(k)$ are given in the Appendix .

Substituting Equations (31) and (32) into the third and forth equations of (25) leads to a system of Fredholm equations of the second kind for $B_1(k)$ and $A_2(k)$:

$$F_{10}(k)+F_{11}(k)B_1(k)+F_{12}(k)A_2(k)$$
$$=\int_{-\infty}^{+\infty}B_1(k')f_{11}(k')g(k,k')dk'+\int_{-\infty}^{+\infty}A_2(k')f_{12}(k')g(k,k')dk' \quad (33)$$

$$F_{21}(k)B_1(k)+F_{22}(k)A_2(k)=\int_{-\infty}^{+\infty}B_1(k')f_{21}(k')g(k,k')dk'$$
$$+\int_{-\infty}^{+\infty}A_2(k')f_{22}(k')g(k,k')dk'+\int_{-\infty}^{+\infty}f_{20}(k')g(k,k')dk' \quad (34)$$

where $F_{10}(k)$, $F_{11}(k)$, $F_{12}(k)$, $F_{21}(k)$, $F_{22}(k)$, $f_{11}(k)$, $f_{12}(k)$, $f_{21}(k)$, $f_{22}(k)$ and $f_{20}(k)$ are given to Appendix. The coupled integral equations are solved numerically using the Nystorm method [14]. The integrals in Equations (33) and (34) are first approximated using Gaussian quadrature with k' evaluated at Gauss nodes k_i and k at k_n . If k_n takes the same values as the Gauss quadrature nodes k_i , then a set of N linear equations of $B_1(k_i)$ and $A_2(k_i)$ for $i=1,2,...,N/2$ is obtained as

$$[C]\begin{bmatrix}B_1(k_1)\\ .\\ B_1(k_{N/2})\\ A_2(k_1)\\ .\\ A_2(k_{N/2})\end{bmatrix}=b \quad (35)$$

where $[C]$ and b are given in the Appendix.

A_2 and B_1 at other wavenumbers than those at the Gauss nodes are calculated using the Nystörm interpolation [14] and the $B_1(k_i)$ and $A_2(k_i)$ obtained though sloving Equation (35). Together with A_1 and B_2 from Equations (31) and (32), they yield the displacements of the foam and the signal conditioning by using Equation (28). Then the radiated sound pressure is calculated by Equation (30) for evaluating the near field sound pressure distribution. Finally the non-dimensional far-field directionality of the sound pressure (using the stationary phase method [15]) is

$$\frac{p(r,\theta)}{\frac{F_o\rho_o}{m\sqrt{2\pi r}}}=\frac{-m\omega^2}{j\sqrt{k_0}}[T^z(k_0\sin\theta)]\begin{bmatrix}A_1(k_0\sin\theta)\\ B_1(k_0\sin\theta)\\ A_2(k_0\sin\theta)\\ B_2(k_0\sin\theta)\end{bmatrix}e^{-jkr+j\pi/4}\ . \quad (36)$$

III. RESULTS AND DISCUSSION

We now demonstrate the significance and mechanisms of the discontinuity introduced by a signal conditioning plate in changing the sound radiation characteristics of the layered plate. The far field directionality and near field pressure distribution at 0.1 and 0.9 of the critical frequencies of the base plate are used for the demonstration. By changing the parameters of the signal conditioning plate, the changes in the far-field and near field radiated sound are observed. We also use the velocity field in the layered plate to explain the wave scattering responsible to the changes in the radiated sound field. The data used for the base plate and elastic foam in the numerical simulations are listed in Table1. The signal conditioning plate is made by steel and its dimentions (thickness h_2 and length L) and offset (x_d) from the centre of the coordinate are given in the subsections and figure captions where they are appropriate. The sound radiation is evaluated at two frequency of the driving force: the lower frequency ($f=0.1f_c$) and the higher frequency ($f=0.9f_c$), where f_c is the coincidence frequency of the in-vacuum base plate.

Table 1. Parameters of the layered plate for simulations

Parameter	Value
Position of the line force x_o	0m
Base plate material	Steel
Coincidence frequency of the base plate f_c	$2.130\times10^4 Hz$
Base plate & foam thickness h & h_1	$0.01m$
Foam density ρ_1	$500kg/m^3$
Foam dilatational wave speed c_d	$150\sqrt{1+j0.1}m/s$
Foam shear wave speed c_s	$50\sqrt{1+j0.3}m/s$

Directionality of far-field sound pressure

Figures 2, 3 and 4 show the directionality of far-field pressure varying with the dimensions and offset of the signal conditioning plate (SCP).

(a) Effect of SCP thickness h_2

For $L=0.4m$ and $x_d=-0.2m$ (symemetric with respect to the origin), as h_2 increases from 0m to $0.02m$, the directionality of the radiated sound at the lower frequency of ($f=0.1f_c$) becomes directional specific ((Figure 2(a)) and is charecterized by three major lobes. At the higher ferquency ($f=0.9f_c$) , the directionality of the layered plate is fea-

tured by two lobes pointing approximately at 45 and 135 degrees with beamwidth of approximately 60 degrees.

(b) Effect of SCP length L

For $h_2 = 0.02m$ and $x_d = -0.2m$, as L increases from 0m to $0.7m$, the gradual change in the directionality at the lower frequency (see Figure 3(a)) is observed. At the higher frequency (Figure 3(b)), $L = 0.4m$ and $L = 0.7m$ yield similar directionality.

(c) Effect of SCP offset x_d

For $h_2 = 0.02m$ and $L = 0.4m$, as the SCP is offset from $-0.2m$ m to $0.6m$, we see the change in the directionality from symmetrical to unsymmetrical. At the low ferquency, the offset increases number of lobes in the directionality, while that at the higher frequency has a specific peak in the directionality indicating a strong spatial interference of the radiated sound due to SCP.

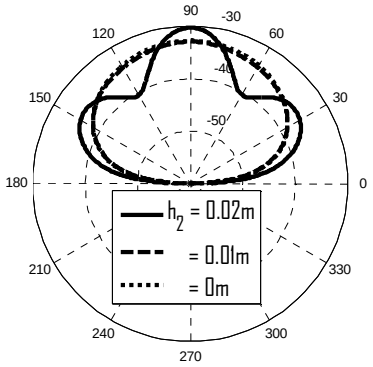

(a)

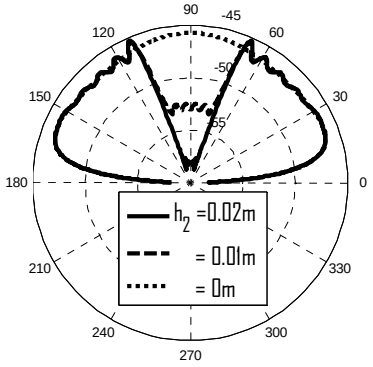

(b)

Figure 2. Nondimensional far-field pressure level of the layered plate varying with h_2. (a) $f = 0.1 f_c$ and (b) $f = 0.9 f_c$.

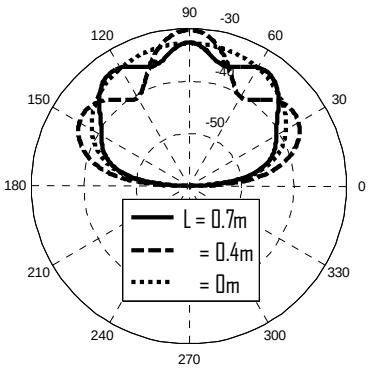

(a)

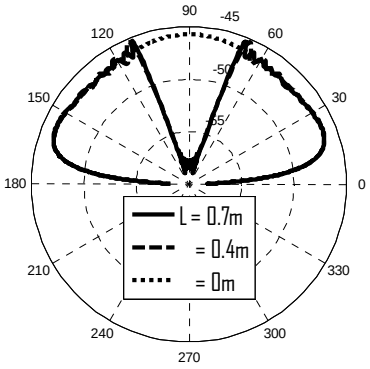

(b)

Figure 3. Nondimensional far-field pressure level of the layered plate varying with L. (a) $f = 0.1 f_c$ and (b) $f = 0.9 f_c$.

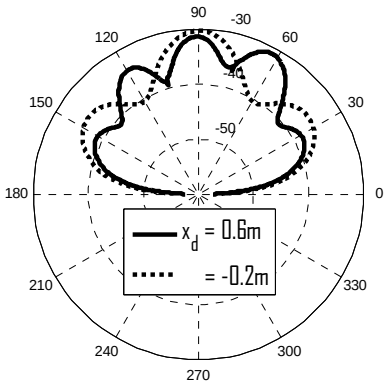

(a)

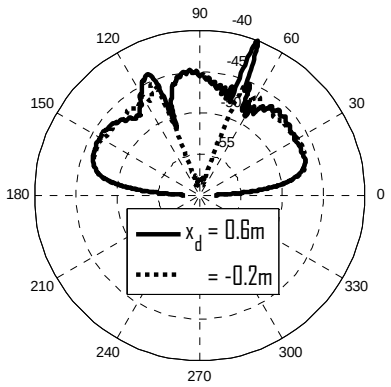

(b)

Figure 4. Nondimensional far-field pressure level of the layered plate varying with x_d . (a) $f = 0.1 f_c$ and (b) $f = 0.9 f_c$.

Near-field sound pressure

Figure 5 shows the near-field sound pressure level from the layered plate without SCP. Non-dimensional spatial locations ($k_p x$ and $k_p z$) are used in the figure to show the spatial distribution of the sound pressure with respect to the wavelength ($2\pi / k_p$) of free bending wave in the invacumm base plate at the excitation frequency. We observed 10dB decay when the distance from the surface doubles at the lower frequency at the near field other than above the driving force location. Above the driving force location, a strong near field component decay slowly over approximately 4 wavelength range is found. The near field sound pressure decays much slower with distance at the higher frequency (see Figure 5(b)). At both frequencies, the localized regions of lower pressure are also found.

(a) Effect of h_2

As a SCP of $h_2 = 0.02m$, $L = 0.4m$ and $x_d = -0.2m$ is placed on the foam, the near field sound pressure in Figure 6(a) becomes much more complicated because of the interference of radiated sound by structural vibration with complicated velocity field especially near the area of the SCP. The fine contours with multiple local structures of near field sound radiation demonstrate the complexity of the hydrodynamic near-field of a vibrating surface with a large range of wavelengths. Figure 6(b) shows the near field when the thickness of SCP is reduced to $0.01m$. For this case, the hydrodynamic near field becomes less complex indicating the surface vibration of the structure becomes less complicated (less participation of structural waves with different wavelengths).

(b) Effect of L

As the length of SCP increases from $0.4m$ to $0.7m$ and other paramenets remain the same as in Figure 6(a), the range of the complexity of the hydrodynamic near field increases (see Figure 6(c). This is expected as the increase size of SCP leads to the extended range of scattering of structural waves.

(c) Effect of x_d

As SCP is located away from the centre of the coordinate to $x_d = 0.6m$ and other paramenets remain the same as in Figure 6(a), the complex strucuture of hydrodynamic near field moves to the location where SCP is. It also changes from symmetric distribution to unsymmetric as expected (see Figure 6(d)).

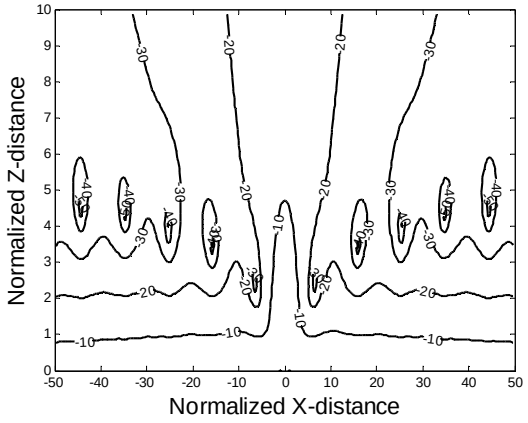

(a)

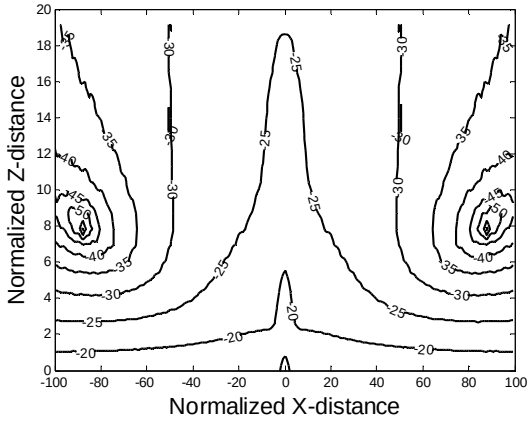

(b)

Figure 5. Near-field sound pressure level of the layered plate without SCP . (a) $f = 0.1 f_c$ and (b) $f = 0.9 f_c$

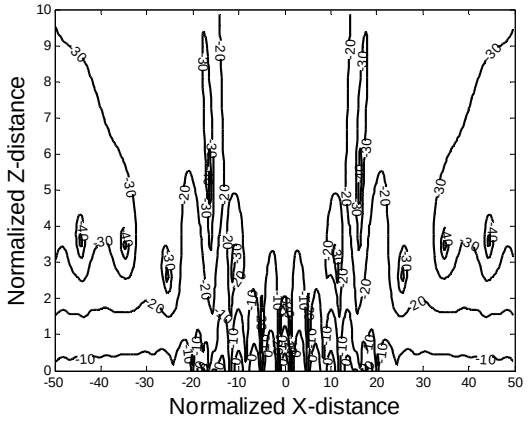

(a)

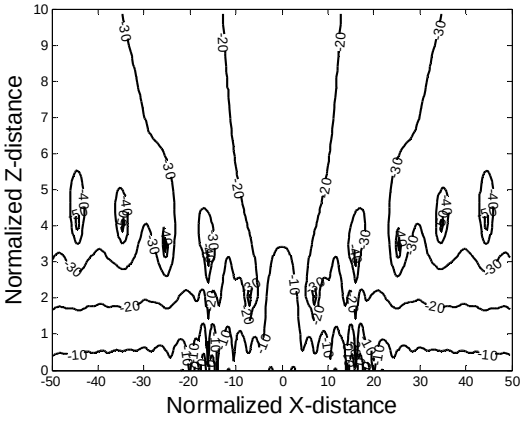

(b)

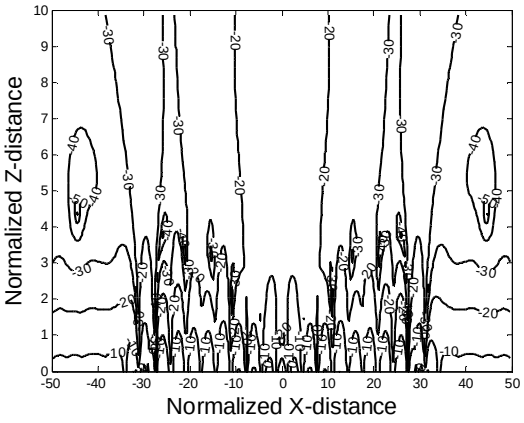

(c)

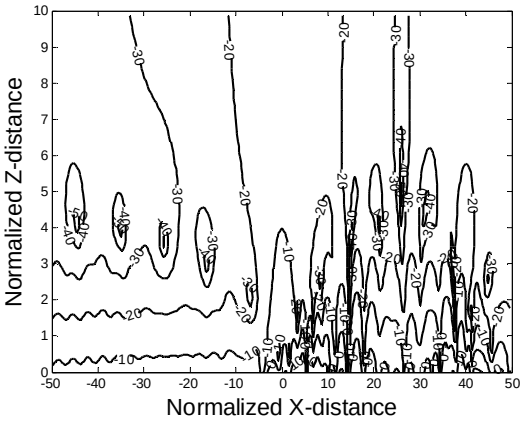

(d)

Figure 6. Near-field sound pressure level of the layered plate with SCP for $f = 0.1 f_c$. (a) $h_2 = 0.02m$, $L = 0.4m$ and $x_d = -0.2m$ (b) $h_2 = 0.01m$, $L = 0.4m$ and $x_d = -0.2m$ (c) $h_2 = 0.02m$, $L = 0.7m$ and $x_d = -0.2m$, and (d) $h_2 = 0.02m$, $L = 0.4m$ and $x_d = 0.6m$.

Similar parametric study of near field sound distributionis is undertaken for higher frequency of $f = 0.9 f_c$. The results of the study are shown in Figure 7. Although we observe the similar complexity in the hydrodynamic near field, the range of the complexity become narrower in the x direction. This is due to the structural waves in the foam that dominate the near field sound are those with shorter wavelengths. This is also expected as the wavelength of scattered wave at higher frequency is shorter.

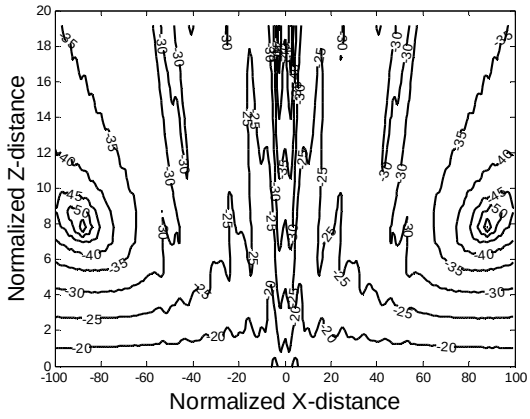

(a)

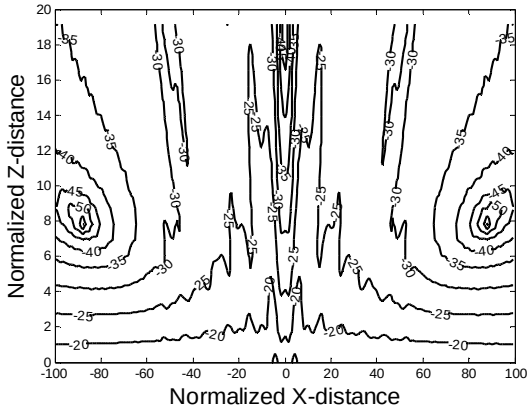

(b)

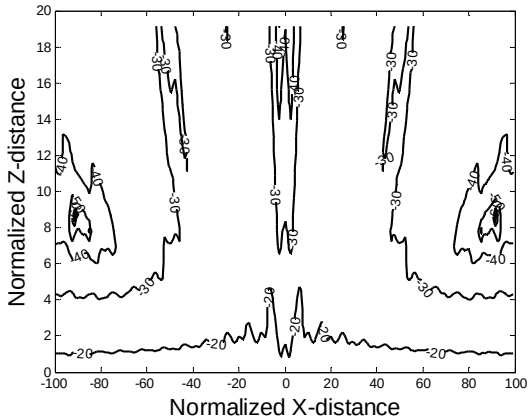

(c)

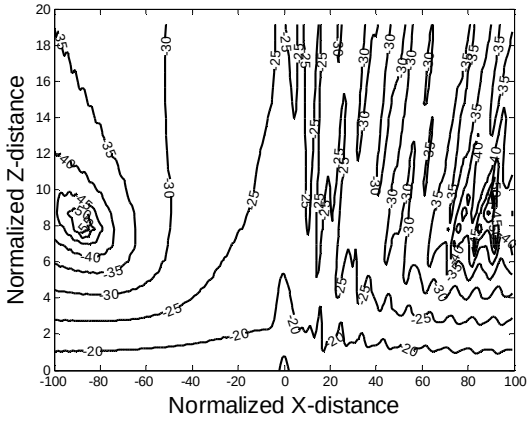

(d)

Figure 7. Near-field sound pressure level of the layered plate with SCP at $f = 0.9 f_c$ (a) $h_2 = 0.02m$, $L = 0.4m$ and $x_d = -0.2m$ (b) $h_2 = 0.01m$, $L = 0.4m$ and $x_d = -0.2m$ (c) $h_2 = 0.02m$, $L = 0.7m$ and $x_d = -0.2m$, and (d) $h_2 = 0.02m$, $L = 0.4m$ and $x_d = 0.6m$.

Velocity field in the foam

To support the explanation of the near field sound distribution presented in Figures 6 and 7, velocity field in the foam is investigated.

(a) Effect of h_2

Shown in Figure 8, as the thickness of the SCP increases, the magnitudes of velocity components on the surface of the layered plate at higher wavenumber also increase. This illustrates the increased range of hydrodynamic near field with the SCP thickness of at $f = 0.1 f_c$. At $f = 0.9 f_c$, the increase of the components at much higher wavenumber (even beyond $k = 200m^{-1}$) is observed and used to explain the small scale complexity of the radiated hydrodynamic near field.

(b) Effect of L

Figure 9 shows the wavenumber spectrum for three different lengthes of SCP. At $f = 0.1 f_c$, the higher wavenumber response for $L = 0.7m$ is lower than that for $L = 0.4m$. On the other hand, the lower wavenumber spectrum for $L = 0.7m$ is higher that that for $L = 0.4m$. This indicats that as the size of the SCP increases the scattered waves are moving towards the longer wavelength direction. The spectrum in Figure 9(b) also shows at $f = 0.9 f_c$, the scattering of the waves with higher wavenumbers is reduced if the length of SCP increases.

(c) Effect of x_d

Offset of SCP from the symmetrical location with respect to the driving force to unsymetrical location causes a significant change in the corresponding wavenumber spectrum of the transverse velocity on the foam surface. The effect of the offset on the spectrum is over the entire wavenumber range at the lower frequency (see Figure 10(a)). Howevere, the changes of the spectrum is only observable in the lower and higher wavenumbers at the higher frequency (see Figure 10(b)).

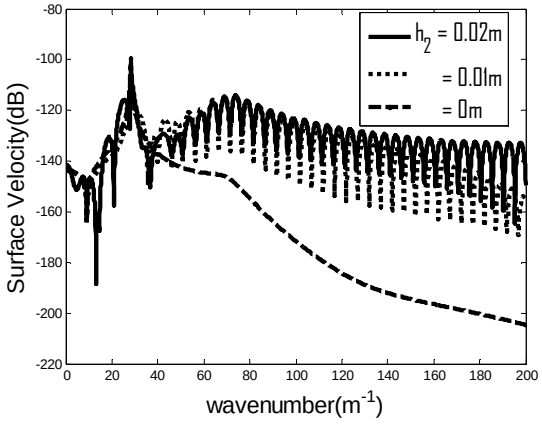

(a)

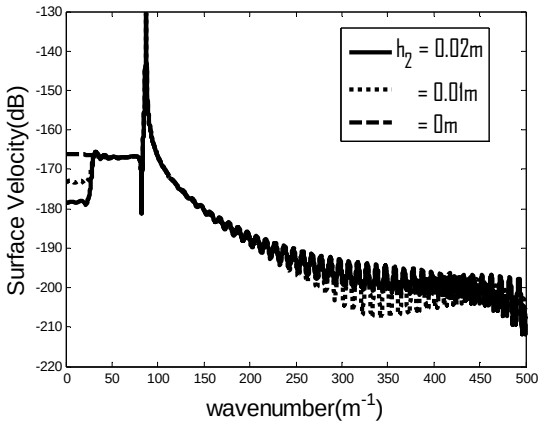

(b)

Figure 8. Velocity spectrum on top of the layered plate varying with h_2 . (a) $f = 0.1 f_c$ and (b) $f = 0.9 f_c$.

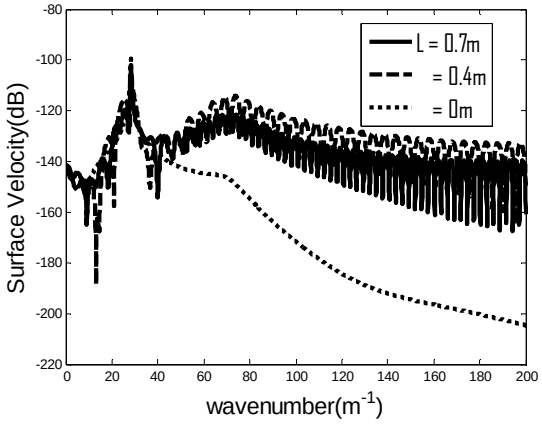

(a)

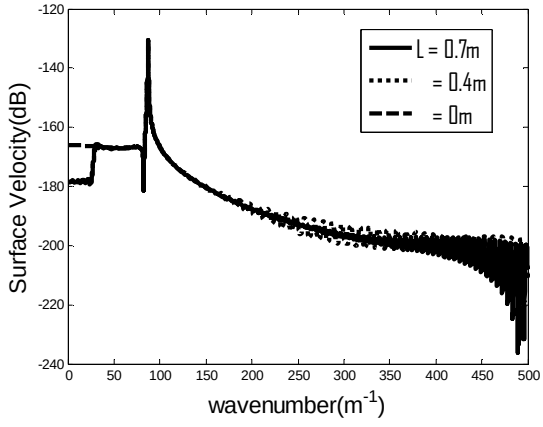

(b)

Figure 9. Velocity spectrum on top of the layered plate varying with L. (a) $f = 0.1 f_c$ and (b) $f = 0.9 f_c$.

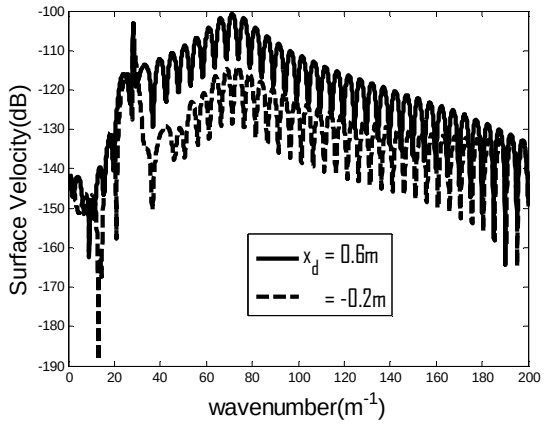

(a)

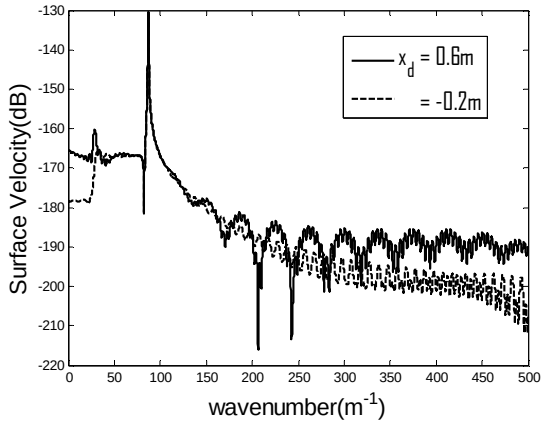

(b)

Figure 10. Velocity spectrum on top of the layered plate varying with x_d. (a) $f = 0.1 f_c$ and (b) $f = 0.9 f_c$.

Finally, we show the normal velocity distribution in the elastic foam in Figures 11 and 12, where the parameters of SCP are $h_2 = 0.02m$, $L = 0.4m$ and $x_d = -0.2m$. With SCP, the low frequency velocity distribution becomes significantly complicated due to strong scattering of the structural waves by SCP (see Figure 11). Howevere, the higher frequency velocity field only have small changes in short wavelength scale when SCP is introduced (see Figure 12). The ratio of size the SCP to the wavelength of the dilatational wave in the foam (L / λ_d) is used for explaining the nature of wave and SCP interaction. At $f = 0.1 f_c$, $L / \lambda_d \approx 6$, while at $f = 0.9 f_c$, $L / \lambda_d \approx 50$. Those ratios indicate that the lower frequency interaction is dominated by the scattering. At the higher frequency, the size of the SCP is much greater than the wavelength. As a result, only refelction and local scattering at the edges of the SCP are important mechanisms in determining the velcoty field.

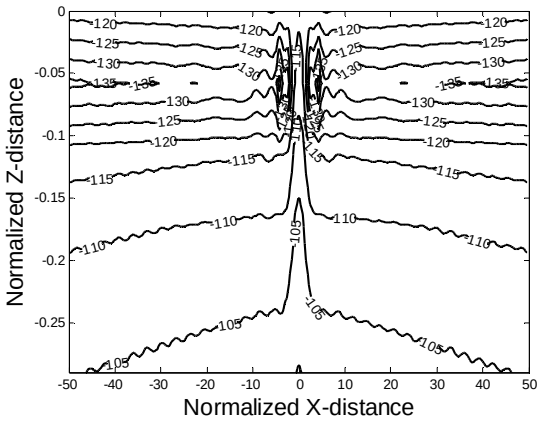

(a)

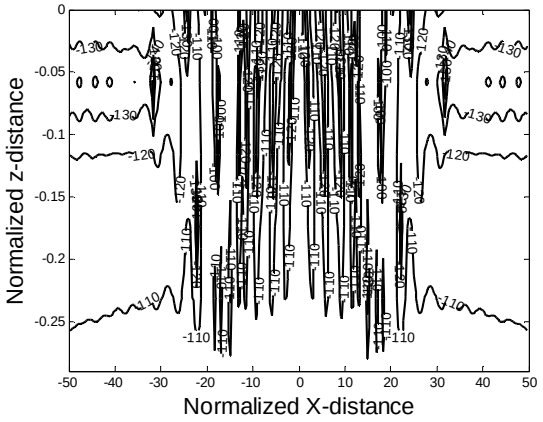

(b)

Figure 11. Normal velcocity field distribution in the foam (in dB) at $f = 0.1 f_c$. (a) without SCP and (b) with SCP.

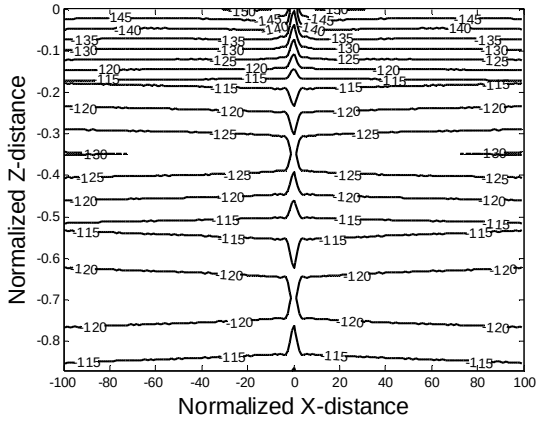

(a)

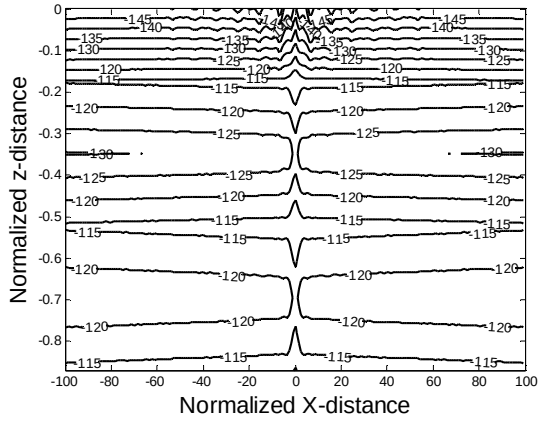

(b)

Figure 12. Normal velcocity field distribution in the foam (in dB) at $f = 0.9 f_c$. (a) without SCP (b) with SCP

IV.SUMMARY AND CONCLUSIONS

An analyticl model is developed for studying sound radiation from a fluid-loaded layered plate with a finite signal conditioning plate on the top. Both far-field directionality and near-field sound pressure distribution are used to demonstrate the effect of the discontinuity introduced by the signal conditioning plate on the sound radiation. The vibration distribution in the elastic foam is also analysed to explain the changes in the radiated sound when the signal conditioning plate is introduced.

Lobe structures are observed in both far-and near-field radiated sound at the two frequencies of investigation (below the coincidence frequency of the base plate) due to the interference between the acoustic waves radiated by structural waves with different wavelength, especially due to (a) scattering waves when the length of the signal conditioning plate is in the same order of magnitude of the elastic wave's wavelength in the foam; (b) reflections of structural waves when the length of SCP is much greater than the wavelengthes.

The thicker the signal conditioning plate is, the stronger the scattering waves are, which leads to stronger lobes in the far-field and inteferece pattern in the near-field.

The offset of the SCP generates the unsymmetrical sound radiation directionality, which indicates the the relative phase angles between the scattered structural waves in the foam significantly controls the interference of the radiated sound.

Although only one thickness of the elastic foam is considered in this simulation, we have found that increasing of the foam thickness mainly reduces the magnitude of system response. The effects of wave interaction with SCP on the far field and near field sound pressure are still observable.

APPENDIX

$$T_{11} = \alpha(D_1 k^4 - \rho h\omega^2)\sin(\alpha h_1) - \rho_1 c_s^2 (k^2 - \beta^2)\cos(\alpha h_1) + \rho_1 c_s^2 k^2 \alpha h \sin(\alpha h_1) \quad \text{(A1a)}$$

$$T_{12} = \alpha(D_1 k^4 - \rho h\omega^2)\cos(\alpha h_1) + \rho_1 c_s^2 (k^2 - \beta^2)\sin(\alpha h_1) + \rho_1 c_s^2 k^2 \alpha h \cos(\alpha h_1) \quad \text{(A1b)}$$

$$T_{13} = -jk(D_1 k^4 - \rho h\omega^2)\cos(\beta h_1) + 2j\rho_1 c_s^2 k\beta \sin(\beta h_1) - jk\frac{h}{2}\rho_1 c_s^2 (k^2 - \beta^2)\cos(\beta h_1) \quad \text{(A1c)}$$

$$T_{14} = jk(D_1 k^4 - \rho h\omega^2)\sin(\beta h_1) + 2j\rho_1 c_s^2 k\beta \cos(\beta h_1) + jk\frac{h}{2}\rho_1 c_s^2 (k^2 - \beta^2)\sin(\beta h_1) \quad \text{(A1d)}$$

$$T_{21} = -2j\rho_1 c_s^2 k\alpha \sin(\alpha h_1) + (\rho h\omega^2 - E_1' h k^2)\cdot \left[-jk\cos(\alpha h_1) - \frac{jkh}{2}\alpha \sin(\alpha h_1)\right] - \frac{jkv_1 h\rho_1 c_s^2 (k^2 - \beta^2)\cos(\alpha h_1)}{2(1 - v_1)} \quad \text{(A1e)}$$

$$T_{22} = -2j\rho_1 c_s^2 k\alpha \cos(\alpha h_1) + (\rho h\omega^2 - E_1' h k^2)\cdot \left[jk\sin(\alpha h_1) - \frac{jkh}{2}\alpha \cos(\alpha h_1)\right] + \frac{jkv_1 h\rho_1 c_s^2 (k^2 - \beta^2)\sin(\alpha h_1)}{2(1 - v_1)} \quad \text{(A1f)}$$

$$T_{23} = -\rho_1 c_s^2 (k^2 - \beta^2)\cos(\beta h_1) + (\rho h\omega^2 - E_1' h k^2)\cdot \left[-\beta \sin(\beta h_1) - \frac{k^2 h}{2}\cos(\beta h_1)\right] - \frac{kv_1 h}{(1 - v_1)}\left[\rho_1 c_s^2 k\beta \sin(\beta h_1)\right] \quad \text{(A1g)}$$

$$T_{24} = \rho_1 c_s^2 (k^2 - \beta^2)\sin(\beta h_1) + (\rho h\omega^2 - E_1' h k^2)\cdot \left[-\beta \cos(\beta h_1) + \frac{k^2 h}{2}\sin(\beta h_1)\right] - \frac{kv_1 h\rho_1 c_s^2 k\beta \cos(\beta h_1)}{(1 - v_1)} \quad \text{(A1h)}$$

$$T_{31} = \rho_1 c_s^2 (k^2 - \beta^2) \quad \text{(A1i)}$$

$$T_{32} = -\frac{\rho_o \omega^2 \alpha}{\alpha_0} \quad \text{(A1j)}$$

$$T_{33} = \frac{jk\rho_o \omega^2}{\alpha_0} \quad \text{(A1k)}$$

$$T_{34} = -2j\rho_1 c_s^2 k\beta \quad \text{(A1l)}$$

$$T_{41} = 0 \quad \text{(A1m)}$$

$$T_{42} = -2j\rho_1 c_s^2 k\alpha \quad \text{(A1n)}$$

$$T_{43} = -\rho_1 c_s^2 (k^2 - \beta^2) \quad \text{(A1o)}$$

$$K_{10} = \frac{T_{24} F \exp(jkx_0)}{T_{11}T_{24} - T_{14}T_{21}} \quad \text{(A2a)}$$

$$K_{11} = \frac{T_{14}T_{22} - T_{12}T_{24}}{T_{11}T_{24} - T_{14}T_{21}} \quad \text{(A2b)}$$

$$K_{12} = \frac{T_{14}T_{23} - T_{13}T_{24}}{T_{11}T_{24} - T_{14}T_{21}} \quad \text{(A2c)}$$

$$K_{20} = \frac{-T_{21} F \exp(jkx_0)}{T_{11}T_{24} - T_{14}T_{21}} \quad \text{(A2d)}$$

$$K_{21} = -\frac{T_{11}T_{22} - T_{12}T_{21}}{T_{11}T_{24} - T_{14}T_{21}} \quad \text{(A2e)}$$

$$K_{22} = -\frac{T_{11}T_{23} - T_{13}T_{21}}{T_{11}T_{24} - T_{14}T_{21}} \quad \text{(A2f)}$$

$$F_{11} = T_{31}K_{11} + T_{34}K_{21} + T_{32} \quad \text{(A2g)}$$

$$F_{12} = T_{31}K_{12} + T_{34}K_{22} + T_{33} \quad \text{(A2h)}$$

$$F_{10} = T_{31}K_{10} + T_{34}K_{20} \quad \text{(A2i)}$$

$$F_{21} = T_{42} \quad \text{(A2j)}$$

$$F_{22} = T_{43} \quad \text{(A2k)}$$

$$f_{11}(k') = \frac{1}{2\pi}[\alpha(\rho_2 h_2 \omega^2 - D_2 k'^4) - k'^2 h_2 \rho_1 c_s^2 \alpha] \quad \text{(A3a)}$$

$$f_{12}(k') = \frac{1}{2\pi}[\frac{jk' h_2 \rho_1 c_s^2 (k'^2 - \beta^2)}{2} - jk'(\rho_2 h_2 \omega^2 - D_2 k'^4)] \quad \text{(A3b)}$$

$$f_{21}(k') = \frac{1}{2\pi}\{(\rho_2 h_2 \omega^2 - E_2' h_2 k'^2)[(\frac{jk' h_2}{2}\alpha - jk' K_{11} - \beta K_{21})] - \frac{jk' \nu_2 h_2}{2(1-\nu_2)}[(\rho_1 c_s^2 (k'^2 - \beta^2) K_{11} - 2j\rho_1 c_s^2 k \beta K_{21} + \frac{\rho_o \omega^2 \alpha}{\alpha_0})\}$$

(A3c)

$$f_{22}(k') = \frac{1}{2\pi}\{(\rho_2 h_2 \omega^2 - E_2' h_2 k'^2)[(\frac{k'^2 h_2}{2} - jk' K_{12} - \beta K_{22}) - \quad \text{(A3d)}$$

$$f_{20}(k') = \frac{1}{2\pi}\{(\rho_2 h_2 \omega^2 - E_2' h_2 k'^2)[-jk' K_{10} - \beta K_{20}]$$

$$-\frac{jk' \nu_2 h_2}{2(1-\nu_2)}[\rho_1 c_s^2 (k'^2 - \beta^2) \cdot K_{10} - 2j\rho_1 c_s^2 k' \beta K_{20}]\} \quad \text{(A3e)}$$

Where $\alpha = \sqrt{k_d^2 - k^2}$ and $\beta = \sqrt{k_s^2 - k^2}$ are the z-directional dilatational and shear wavenumber, respectively. k_d and k_s are the x-directional dilational and shear wave number, respectively. c_d and c_s are the dilatational and shear wave speeds, respectively.

$$C = \begin{bmatrix} \overrightarrow{F_{11}} - \overrightarrow{R_{11}} & \overrightarrow{F_{12}} - \overrightarrow{R_{12}} \\ \overrightarrow{F_{21}} - \overrightarrow{R_{21}} & \overrightarrow{F_{22}} - \overrightarrow{R_{22}} \end{bmatrix} \quad \text{(A4a)}$$

$$b = \begin{bmatrix} -\overrightarrow{F_{10}} \\ \overrightarrow{R_{20}} \end{bmatrix} \quad \text{(A4b)}$$

where

$$\overrightarrow{F_{11}} = diag(F_{11}(k_i)) \quad \text{(A4c)}$$

$$\overrightarrow{F_{12}} = diag(F_{12}(k_i)) \quad \text{(A4d)}$$

$$\overrightarrow{F_{21}} = diag(F_{21}(k_i)) \quad \text{(A4e)}$$

$$\overrightarrow{F_{22}} = diag(F_{22}(k_i)) \quad \text{(A4f)}$$

$$\overrightarrow{F_{20}}(k_i) = F_{20}(k_i) \text{ (Column vector)} \quad \text{(A4g)}$$

$$\overrightarrow{R_{11}}(k_n, k_i) = \sum_i^{N/2} \lambda_i f_{11}(k_i) g(k_n, k_i) \quad \text{(A4h)}$$

$$\overrightarrow{R_{12}}(k_n, k_i) = \sum_i^{N/2} \lambda_i f_{12}(k_i) g(k_n, k_i) \quad \text{(A4i)}$$

$$\overrightarrow{R_{21}}(k_n, k_i) = \sum_i^{N/2} \lambda_i f_{21}(k_i) g(k_n, k_i) \quad \text{(A4j)}$$

$$\overrightarrow{R_{22}}(k_n, k_i) = \sum_i^{N/2} \lambda_i f_{22}(k_i) g(k_n, k_i) \quad \text{(A4k)}$$

$$\overrightarrow{R_{20}}(k_n) = \sum_i^{N/2} \lambda_i f_{20}(k_i) g(k_n, k_i) \text{ (Column vector)} \quad \text{(A4l)}$$

where

$$\overrightarrow{f_{11}} = diag(f_{11}(k_i)) \quad \text{(A4m)}$$

$$\overrightarrow{f_{12}} = diag(f_{12}(k_i)) \quad \text{(A4n)}$$

$$\overrightarrow{f_{21}} = diag(f_{21}(k_i)) \quad \text{(A4o)}$$

$$\overrightarrow{f_{22}} = diag(f_{22}(k_i)) \quad \text{(A4p)}$$

$$\overrightarrow{f_{20}}(k_i) = f_{20}(k_i) \text{ (Column vector)} \quad \text{(A4q)}$$

$$\vec{g} = diag(g(k_i, k_n)) \quad \text{(A4r)}$$

REFERENCES

1 S.H. Ko, “Reduction of structure-borne noise using an air-voided elastomer”. *J. Acoust. Soc. Am.* **101**(6), 3306-3312 (1997)

2 R. F. Keltie, “Signal response of elastically coated plates”. *J. Acoust. Soc. Am.* **103**(4), 1855-1863 (1998)

3 O. Foin, A. Berry and J. Szabo, “Acoustic radiation from an elastic baffled rectangular plate covered by a decoupling coating and immersed in a heavy acoustic fluid”. *J. Acoust. Soc. Am.* **107**, 2501-2510 (2000)

4 A. Berry, O. Foin and J.P. Szabo, “Three-dimensional elasticity model for a decoupling coating on a rectangular plate immersed in a heavy fluid”. *J. Acoust. Soc. Am.* **109**(6), 2704-2714 (2001)

5 C. Seren and S.I. Hayek, “Acoustic radiation from an insonified elastic plate with a line discontinuity”. *J. Acoust. Soc. Am.* **86** (1), 195–209(1989)

6 A.G. Pathak and P.R. Stepanishen, “Acoustic harmonic plane wave scattering from infinite elastic plates with a line impedance discontinuity”. *J. Acoust. Soc. Am.* **94**(3), 3428-3436(1993)

7 J.M. Cuschieri and D. Feit, “A hybrid numerical and analytical solution for the Green's function of a fluid-loaded elastic plate”. *J. Acoust. Soc. Am.* **95**(4), 1998-2005 (1994)

8 D. Feit and J.M. Cuschieri, ‘‘Scattering of sound by a fluid-loaded plate with a distributed mass-inhomogeneity’’. *J. Acoust. Soc. Am.* **99**, 2686–2700 (1996)

9 J. M. Cuschieri and D. Feit, ''Full numerical solution for the far field and near field scattering from a fluid-loaded elastic plate with distributed mass or stiffness inhomogeneity''. *J. Acoust. Soc. Am.* **104**, 915–925 (1998)
10 D.T. DiPerna and D. Feit, "A perturbation technique for the prediction of the displacement of a line-driven plate with discontinuities". *J. Acoust. Soc. Am.* **107**(4), 2004-2010 (2000)
11 S.S. Tavallaey, "Wave Propagation in Sandwich Structures", *Doctoral Thesis*, (KTH, Stockholm, 2001) pp.8-9
12 L. Cremer and M. Heckl, *Structure-borne Sound: Structural Vibration and Sound Radiation (2nd Ed.)*, (Springer-Verlag, Berlin, 1998) pp.172
13 S.H. Ko, S. Pyo and W. Seong, *Structure-Borne and Flow noise Reductions (Mathematical Modeling).* (Seoul National University Press, Seoul, Korea, 2001) pp.149-151
14 K.E. Atkinson. *A Survey of Numerical Methods for the Solution of Fredholm Integral Equations of the Second Kind.* (SIAM, Philadelphia, 1976) pp.89
15 M.C. Junger and D. Feit, *Sound, structures, and their interaction (2nd edition).* (Cambridge, MA, MIT Press, 1986) pp.103